Supplementary Information

Facile Synthesis of Self-Supported Mn_3O_4@C Nanotube Arrays Constituting an Ultrastable and High-Rate Anode for Flexible Li-Ion Batteries

*Bin Lu[a,b], Jun Liu[a,b], Renzong Hu[a,b], Hui Wang[a,b], Jiangwen Liu[a,b], Min Zhu[a,b,]**

[a]School of Materials Science and Engineering, Key Laboratory of Advanced Energy Storage Materials of Guangdong Province, South China University of Technology, Guangzhou, 510641, China

[b]China-Australia Joint Laboratory for Energy & Environmental Materials, South China University of Technology, Guangzhou, 510641, China

* Corresponding author

E-mail address: memzhu@scut.edu.cn

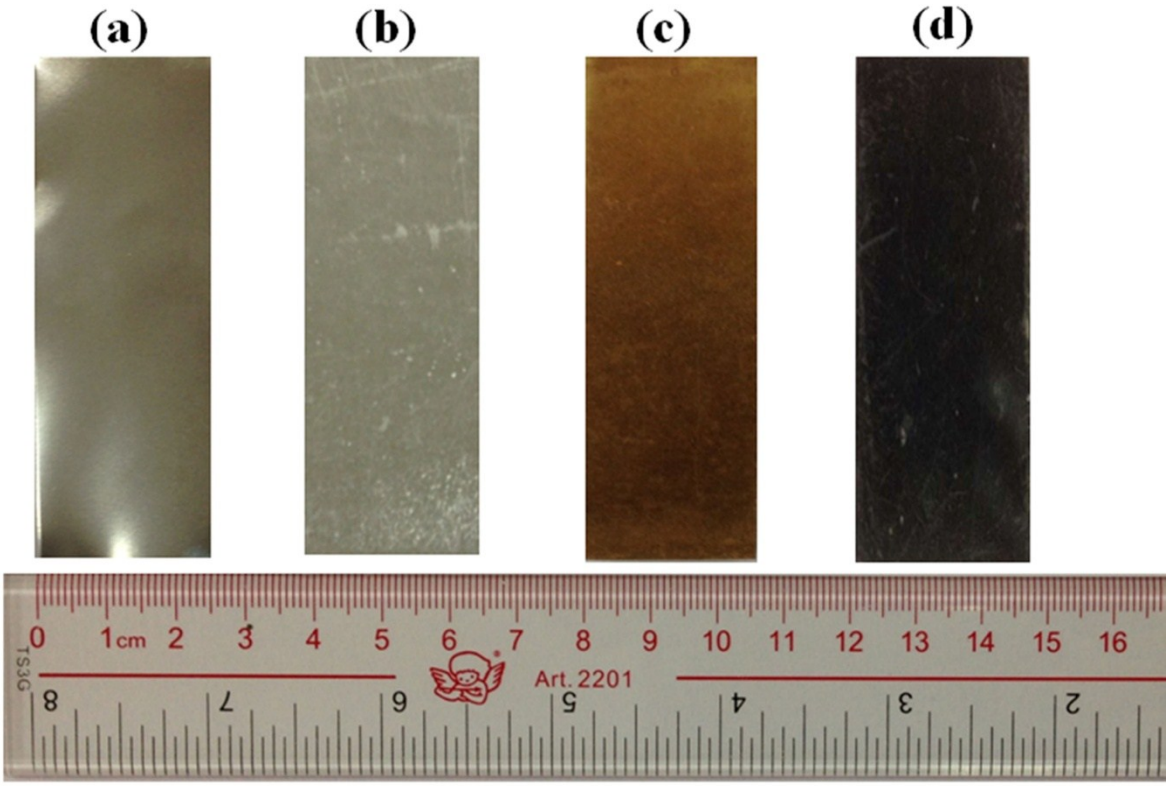

Figure S1. Optical photographs of pure stainless steel foil (a), stainless steel foil grown with ZnO nanorod arrays (NRAs) (b), stainless steel foil grown with ZnO@MnO_2 NRAs (c), and stainless steel foil grown with Mn_3O_4@C nanotube arrays (d).

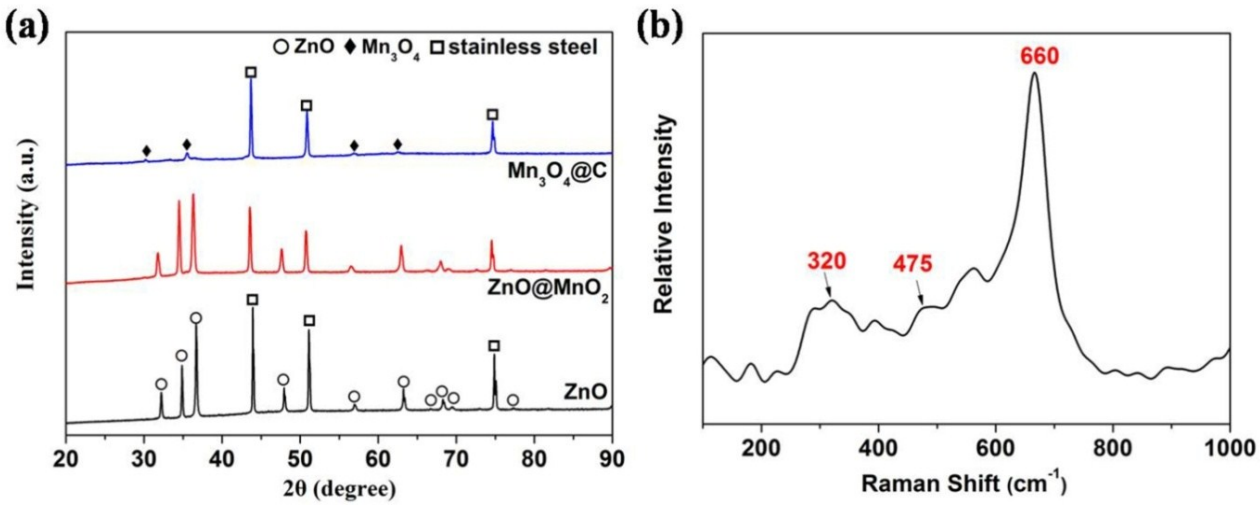

Figure S2. (a) XRD patterns of crystallized ZnO NRAs, ZnO@MnO_2 NRAs and Mn_3O_4@C nanotube arrays on stainless steel foil. The main diffraction peaks of ZnO NRAs and Mn_3O_4 nanotube arrays match well with hexagonal ZnO (JCPDS No. 36-1451) and hausmannite Mn_3O_4 phase (JCPDS No. 24-0734), respectively. (b) Raman spectrum of the Mn_3O_4@C nanotube arrays.

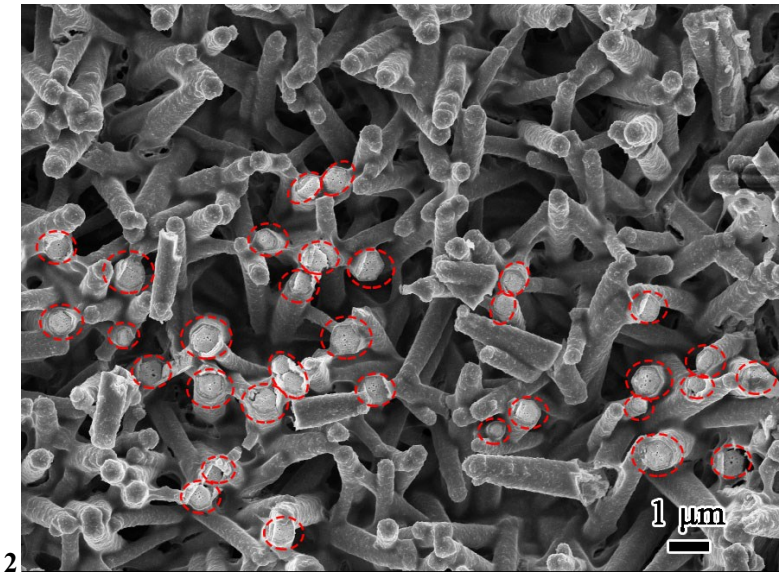

Figure S3. Surface SEM image of ZnO@Mn_3O_4@C NRAs on steel substrate. Some top-end of the ZnO@Mn_3O_4@C NRAs (red dash cycles) are without Mn_3O_4.

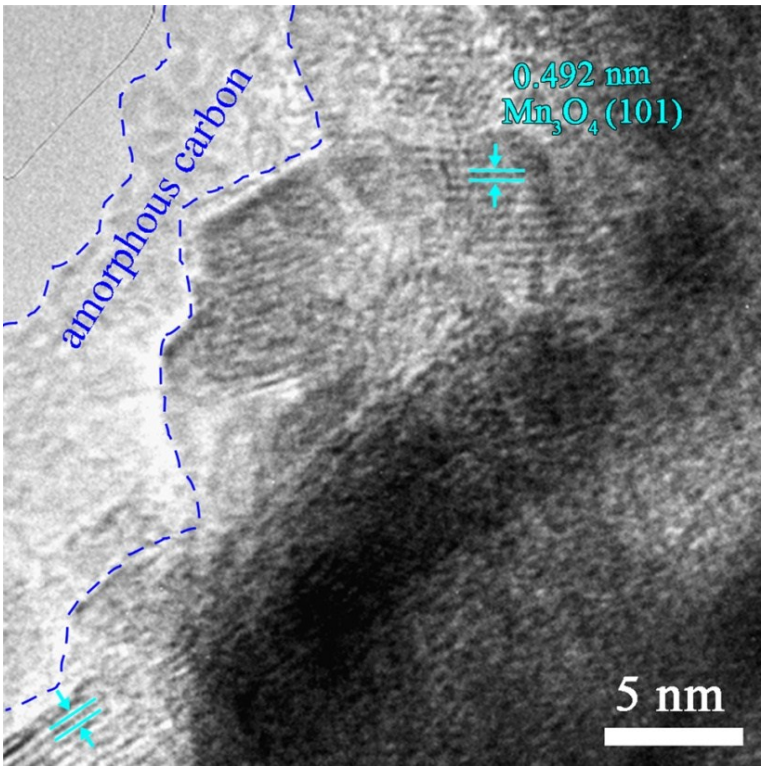

Figure S4. More HRTEM image of a typical Mn_3O_4@C nanotube. It clearly shows the amorphous carbon coated on the surface of Mn_3O_4 nanotube.

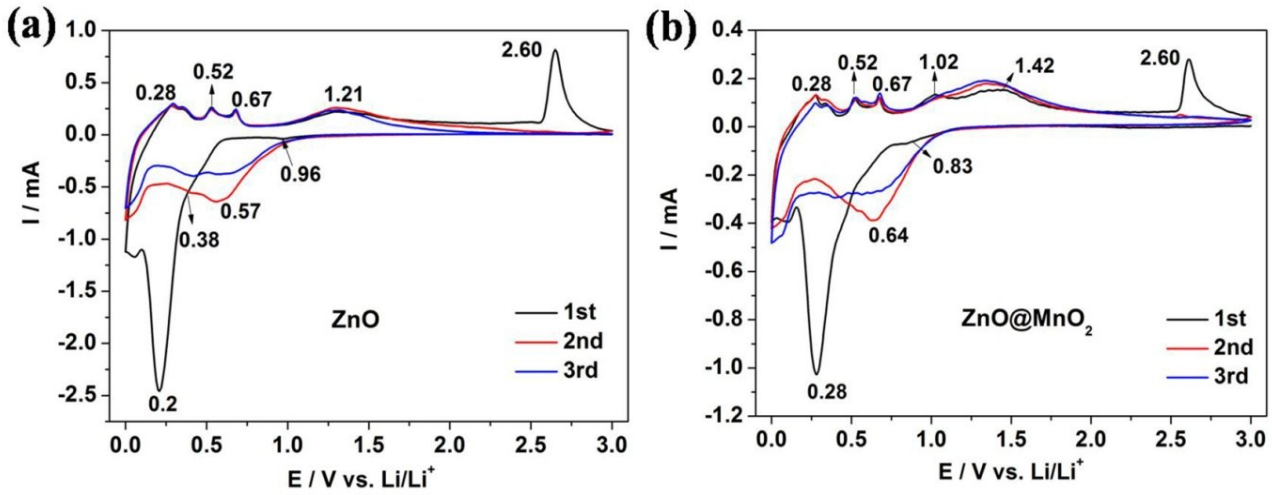

Figure S5. CV curves for (a) ZnO NRAs, (b) ZnO@MnO_2 NRAs from 0.0 to 3.0 V *vs.* Li^+/Li at scanning rate of 0.2 mV s^{-1}.

Figure S5a and S5b display the first three CV profiles of ZnO and ZnO@MnO_2 NRAs from 0.0 to 3.0 V *vs.* Li^+/Li, respectively. In the cathodic process, the reduction peaks at 0.96 V (Figure S5a) and 0.83 V (Figure S5b) are ascribed to the irreversible formation of the SEI film.[1,5] The lithiation peak at 0.2V (Figure S5a) in the first cycle is corresponded to the reductive reaction of ZnO to Zn and further alloying with Li,[2] which is divided into two peaks located at 0.38 and 0.57 V in the followed cycles. While in Figure S5b, the lithiation peak at 0.28 V is assigned to the reduction of ZnO and MnO_2 and Zn further alloying with Li,[1,5] which shifts to 0.64V afterwards. In the anodic process, the delithiation peaks located at 0.28, 0.52, 0.67, 1.21 V in Figure S5a and peaks at 0.28, 0.52, 0.67, 1.42 V in Figure S5b are attributed to the de-alloying process of LiZn.[3,4] The delithiation peak at 1.02 V in figure S5b is related to the oxidation of Mn.[5] Furthermore, the high oxidation peak at 2.60 V in both Figure S5a and S5b is assigned to the oxidation of Zn to ZnO,[2] which is the featured peak of the existence of ZnO. The above related reactions could be depicted as below:

$$ZnO + 2Li^+ + 2e^- \leftrightarrow Zn + Li_2O \quad (1)$$

$$Zn + Li^+ + e^- \leftrightarrow LiZn \quad (2)$$

$$MnO_2 + 4Li^+ + 4e^- \leftrightarrow 2Li_2O + Mn \quad (3)$$

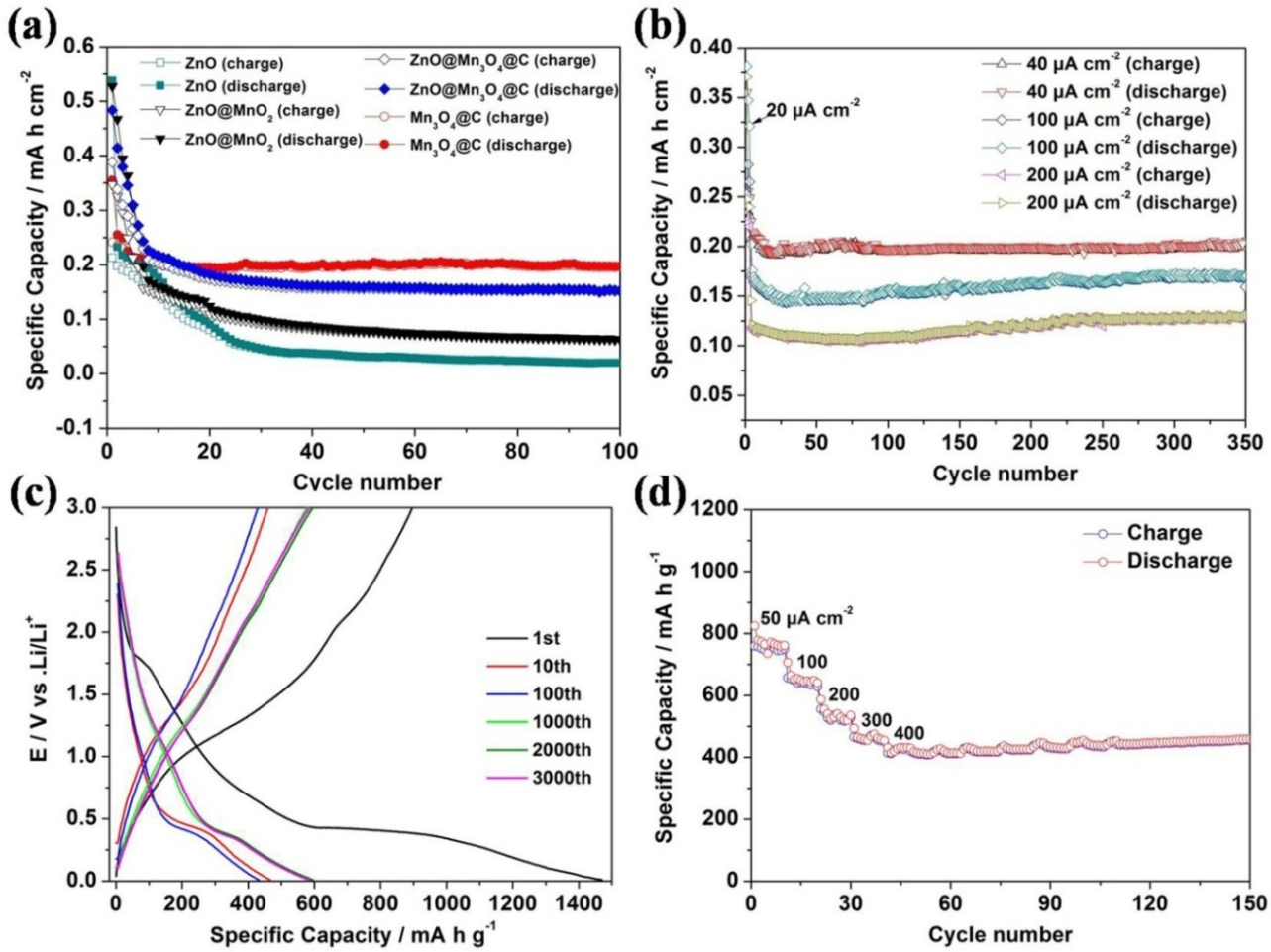

Figure S6. (a) Comparison of cyclic performance for ZnO, ZnO@MnO_2, ZnO@Mn_3O_4@C, Mn_3O_4@C composite electrodes from 0.01 to 3.0 V *vs*. Li^+/Li at 40 μA cm^{-2}, the first three cycles were activated at 20 μA cm^{-2}. (b) Cycle performance at different current rates (40, 100, 200 μA cm^{-2}) between 0.01 and 3.0 V, the first three cycles were activated at 20 μA cm^{-2}. (c) The discharge-charge curves of Mn_3O_4@C nanotube arrays at current rate of 200 μA cm^{-2}/793 mA g^{-1} between 0.01 and 3.0 V. (d) Rate capability of Mn_3O_4@C nanotube arrays electrode with a current density range from 50 to 400 μA cm^{-2} after three activation cycles, cut off potential: 0.01–3 V *vs.* Li^+/Li.

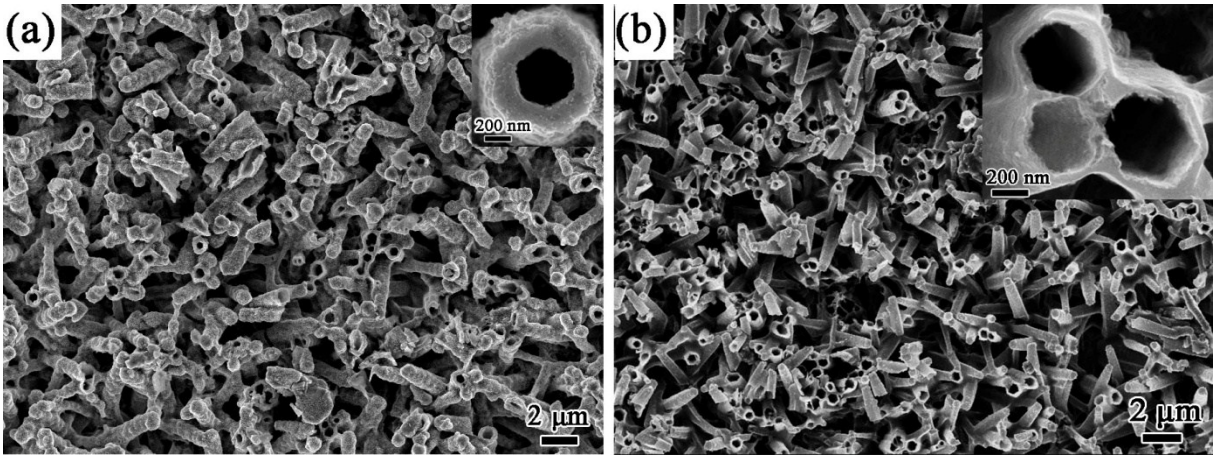

Figure S7. SEM micrographs of Mn_3O_4@C nanotube arrays with different loading densities: (a) 0.48 mg cm^{-2}, (b) 0.25 mg cm^{-2}. The Mn_3O_4@C with the loading density of 0.25 mg cm^{-2} (denoted as 0.25-Mn_3O_4@C) was synthesized according to the manuscript. While the Mn_3O_4@C with a higher loading density of 0.48 mg cm^{-2} (denoted as 0.48-Mn_3O_4@C) composite was prepared by prolonging the MnO_2 deposition from 4h to 6h and increased the glucose concentration from 0.4 M to 0.6 M. (The weight of Mn_3O_4@C nanotube arrays on stainless steel substrate was calculated based on the mass difference of the stainless steel substrate before and after the growth of Mn_3O_4@C nanotube arrays).

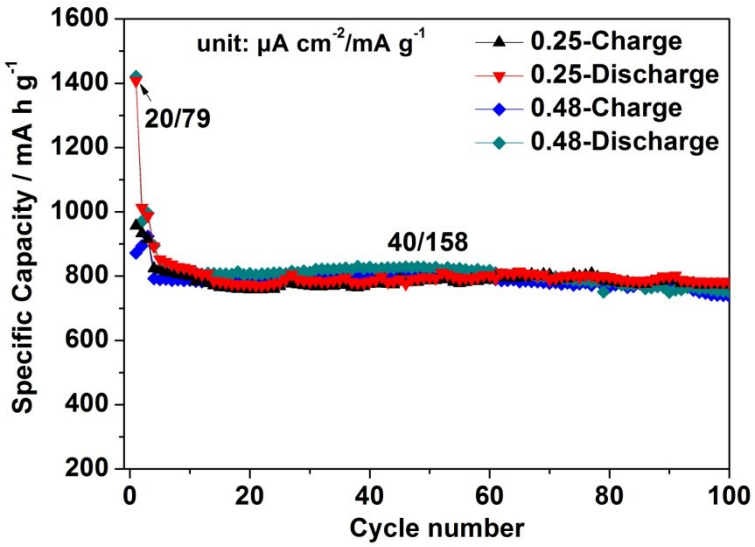

Figure S8. Cyclic performance of Mn_3O_4@C electrodes with loading densities of 0.25 and 0.48 mg cm^{-2} (denoted as 0.25-Mn_3O_4@C and 0.48-Mn_3O_4@C, respectively) at 40 μA cm^{-2}/158 mA g^{-1} between 0.01 and 3.0 V *vs.* Li/Li^+ after three cycles activation at 20 μA cm^{-2}/79 mA g^{-1}. The 0.25-Charge and 0.25-Discharge represent the cyclic performance curves of 0.25-Mn_3O_4@C electrode. The 0.48-Charge and 0.48-Discharge represent the cyclic performance curves of 0.48-Mn_3O_4@C electrode.

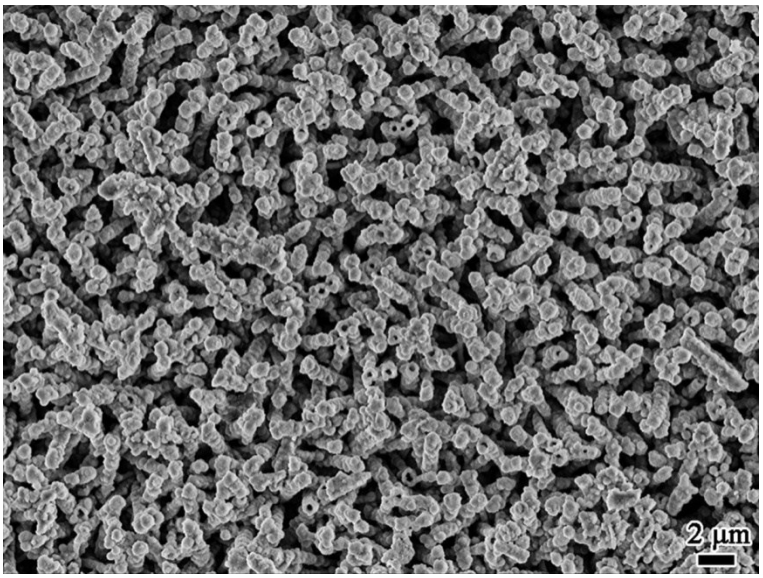

Figure S9. Low-resolution SEM image of Mn_3O_4@C nanotube arrays on substrate after 3000 cycles at 200 μA cm^{-2}/793 mA g^{-1}.

Table S1. Summary of the representative Mn_3O_4-based anode materials for Li-ion batteries.

Materials	**Struture**	**Reversible Capacity (mA h g^{-1})/Cycles or rate**	**Current density (mA g^{-1})**	**Ref.**
Mn_3O_4–graphene	Nanoparticles	600/500th 550 (rate) 400 (rate)	800 1600 4000	[18]
Mn_3O_4/graphene	Nanorod	573/100th 411 (rate) 313 (rate) 196 (rate)	100 500 1000 2000	[26]
Mn_3O_4/graphene	Nanowires	702/100th 550 (rate) 450 (rate) 308 (rate)	100 500 1000 2000	[23]
Mn_3O_4/graphene	Mesoporous particles	540/100th 460 (rate) 320 (rate) 180 (rate)	80 400 800 1600	[21]
Mn_3O_4/graphene	Nanobead	1100/240th 600 (rate) 500 (rate) 415 (rate) 320 (rate)	100 200 300 500 1000	[36]
Mn_3O_4/graphene	Nanoparticle	500/40th 390 (rate) 200 (rate)	60 250 1500	[22]
Mn_3O_4/MWCNTs	Nanoparticle	592/50th 585 (rate) 500 (rate) 387 (rate)	100 250 500 1000	[17]
Mn_3O_4/CNT	Nanoparticle	380/100th 490 (rate) 460 (rate) 440 (rate) 400 (rate)	936 468 936 1872 4680	[29]
Mn_3O_4@C	Nanorod	473/50th	40	[12]
Mn_3O_4/reduced GO	Nanoparticles	730/40th 390 (rate)	400 1600	[19]

Mn_3O_4/mesoporous carbon	Nanoparticle	780/50th	100	[20]
Mn_3O_4	Octahedra	746/300th 620/300th	100 300	[9]
Mn_3O_4	Mesoporous nanotubes	641/100th 525 (rate)	500 1000	[16]
Mn_3O_4	Spongelike nanoparticles	800/40th	30	[10]
Mn_3O_4@C	Nanotube arrays	785/350th 635/350th 590/3000th 460 (rate) 420 (rate) 400 (rate) 375 (rate)	158 396 793 1189 1586 1982 2380	Our work

Reference

1 G. Gachot, S. Grugeon, M. Armand, S. Pilard, P. Guenot, J.-M. Tarascon and S. Laruelle, *J. Power Sources*, 2008, **178**, 409-421.

2 X. Huang, X. Xia, Y. Yuan and F. Zhou, *Electrochim. Acta*, 2011, **56**, 4960-4965.

3 F. Belliard and J. Irvine, *J. Power Sources*, 2001, **97**, 219-222.

4 J. Liu, Y. Li, X. Huang, G. Li and Z. Li, *Adv. Funct. Mater.*, 2008, **18**, 1448-1458.

5 J. Fang, Y. Yuan, L. Wang, H. Ni, H. Zhu, J. Yang, J. Gui, Y. Chen and S. Guo, *Electrochim. Acta*, 2013, **112**, 364-370.